Journal of Nuclear Medicine, published on September 27, 2019 as doi:10.2967/jnumed.119.231845

PennPET Explorer: Human Imaging on a Whole-body Imager

Austin R. Pantel[1], Varsha Viswanath[2], Margaret E. Daube-Witherspoon[1], Jacob G. Dubroff[1], Gerd Muehllehner[3], Michael J. Parma[1], Daniel A. Pryma[1], Erin K. Schubert[1], David A. Mankoff[1], Joel S. Karp[1]

[1] Department of Radiology, University of Pennsylvania, Philadelphia, PA
[2] Department of Biomedical Engineering, University of Pennsylvania, Philadelphia, PA
[3] KAGE Medical, Wayne, PA

Financial support:

We acknowledge support from NIH R01-CA206187, R33-CA225310, R01-CA113941, and KL2TR001879. We also acknowledge support from Philips Healthcare and the Department of Radiology, University of Pennsylvania.

Author responsible for correspondence:

Joel S. Karp, Ph.D.
3620 Hamilton Walk, 154 John Morgan Building
University of Pennsylvania
Philadelphia, PA 19104
(215) 573-4998
fax: (215) 573-3880
joelkarp@pennmedicine.upenn.edu

Total # words: 5782

Running title: PennPET Explorer human imaging

ABSTRACT:

The PennPET Explorer, a prototype whole-body imager currently operating with a 64-cm axial field-of-view (FOV), can image the major body organs simultaneously with higher sensitivity than that of commercial devices. We report here the initial human imaging studies on the PennPET Explorer with each study designed to test specific capabilities of the device. We demonstrate the ability to scan for shorter duration, or, alternatively with less activity, without a compromise in image quality. Delayed images, up to 10 half-lives with FDG, reveal biological insight and support the ability to track biologic processes over time. In one clinical patient, the PennPET Explorer better delineates extent of ^{18}F-fluorodeoxyglucose (FDG)-avid disease. In a second clinical study with ^{68}Ga-DOTATATE we demonstrate comparable diagnostic image quality on the PennPET compared to the clinical scan, but with one-fifth the activity. Dynamic imaging studies capture relatively noise-free input functions for kinetic modeling approaches. Additional studies with experimental research radiotracers illustrate the benefits from the combination of large axial coverage and high sensitivity. These studies provide proof-of-concept for many proposed applications for a long axial FOV PET scanner.

Key words: Positron Emission Tomography, whole-body imager, human imaging

INTRODUCTION

Molecular imaging with positron emission tomography (PET) offers the unique ability to noninvasively interrogate biologic processes through the detection of emitted photons from an administered radiotracer. Although technological advances in the development of modern PET scanners have enabled the acquisition of diagnostic-quality images in under 10 min, these instruments remain inherently inefficient. Limited by a standard axial field-of-view (FOV) of less than 26 cm, commercial PET scanners detect about ~1% of emitted photons and need to move through several bed positions to capture relevant anatomy (*1-3*). To overcome these inherent limitations of standard axial FOV PET scanners, a team of investigators has come together to develop whole-body PET imaging devices as the EXPLORER consortium *(4,5)*. As part of this effort, we have developed the PennPET Explorer, a whole-body PET imager *(6)*.

Whole-body PET imagers provide unique advantages over commercial state-of-the-art PET scanners. With an extended axial FOV, sensitivity increases and detection of isotropically emitted photons from a larger detection area is more likely. The increased sensitivity could be leveraged for shorter scans or, alternatively, a decreased administered activity without a compromise in image quality. While the tradeoff between administered activity and image quality is well established, the dramatic increase in sensitivity afforded by a whole-body PET imager opens the door to previously unthinkable possibilities such as PET images with essentially negligible radiation exposure or dynamic imaging of the whole body with high temporal resolution. Imaging isotopes like ^{68}Ga, whose activity is often limited by generator production, or delayed imaging with longer-lived isotopes like ^{18}F to study late kinetics (*7*), becomes feasible. Even more delayed imaging can be obtained for longer-lived radiotracers, such as ^{89}Zr, to study slower biological processes including dosimetry and cell tracking applications, despite its low positron yield. Whole-body coverage enables kinetic analysis of

lesions outside a standard axial FOV and ensures the inclusion of large vascular structures for input functions. Finally, the potential for rapid imaging with low administered activities could enable the consideration of PET utilization in a broad spectrum of diseases not currently interrogated with PET. These expanded capabilities have both research and direct clinical applications (*4,5*).

To develop whole-body PET imagers and realize the benefits of such a device, the EXPLORER Consortium was formed in 2015. Two large axial FOV PET scanners have been borne out of this program: a 194-cm scanner developed by the UC Davis team in collaboration with United Imaging Healthcare (Shanghai, China) and a scanner developed at the University of Pennsylvania in collaboration with KAGE Medical (Wayne, PA) and Philips Healthcare (Cleveland, Ohio). The first human studies of the former system have been previously published (*8*). High-quality images were seen in a series of four normal volunteers; the ability to image with a lower administered activity and at later time points was also explored. Herein, we discuss the first human studies of the second system, the PennPET Explorer, a prototype whole-body imager in a three-ring configuration operating with a 64-cm axial FOV, which will soon be expanded to 140-cm axial FOV.

In these initial human studies of the PennPET Explorer, hereafter referred to as PennPET, we sought to progressively test the capabilities of this whole-body imager. We first imaged healthy subjects, then clinical patients with disease, and finally research subjects. Imaging protocols were tailored to study the performance of the PennPET in the context of specific clinical and research questions matched to the subject and radiotracer. This study was designed to demonstrate how the sensitivity of the whole-body imager can be leveraged to benefit specific applications depending on the particular imaging need. The prototype configuration has sufficient axial coverage to demonstrate proof-of-concept of the benefits of a long axial FOV,

although the expansion of the system beyond its current axial length will permit simultaneous imaging of all major organs with adequate sensitivity at the extremities.

MATERIALS AND METHODS

Scanner Characteristics

The general design of the PennPET Explorer whole-body imager has been previously described (*9,10*). Our companion paper provides additional details and describes initial testing of the system, performance measurements, and optimization for human imaging (*6*). Here, we briefly summarize the salient characteristics. The prototype configuration has three rings and an axial FOV of 64 cm. The instrument is based on a digital silicon photomultiplier (dSiPM) developed by Philips Digital Photon Counting (PDPC) (*11*) with 1:1 crystal coupling, high count rate capability (noise equivalent count rate (NECR) > 1000 kcps at 40 kBq/cc), and a 250-ps timing resolution. With three rings we achieve a sensitivity of 55 kcps/MBq, about nine times greater than that of a single ring. Other salient performance measures include a spatial resolution of 4.0 mm and energy resolution of 12%.

Image Reconstruction

All data are acquired in singles list-mode format and sorted into a list of coincidence events; randoms are estimated from the delayed events, scatter is estimated using time-of-flight (TOF) single-scatter simulation (SSS) (*12*) and the data are reconstructed using TOF list-mode (LM) ordered subsets expectation maximization (OSEM) (*13*) (25 subsets) into 2-mm isotropic voxels for the body and a 576-mm transverse field-of-view. The list-mode algorithm includes optimized basis functions to suppress image noise while preserving signal, hence no post-filtering is used.

To facilitate a direct comparison with the PennPET data for the first subject, the standard of care (SOC) data from the clinical PET/CT system were reprocessed with the same reconstruction tools as used for the corresponding PennPET data. However, for the two clinical scans

presented, the SOC data were reconstructed with a smoother basis function and into 4-mm^3 voxels as used in the clinic, rather than 2-mm^3 used for the PennPET reconstruction.

For these proof-of-concept studies presented, the CT scan from the comparator commercial PET/CT was used for attenuation correction, but was not required for anatomic localization. Clinical patients were scanned with their arms up; all other patients were scanned with their arms down. Commercial software (MIM Software, Inc., Cleveland, OH) was used to perform a rigid-body registration between the non-attenuation corrected (NAC) PET images from the PennPET and the CT image, which was then transformed and projected to form the attenuation correction factors. To aid in the alignment, a flat pallet with indexing marks was used for most scans to facilitate reproducible subject positioning and permit the use of rigid-body registration. The flat pallet was not used for the two clinical scans, although the registration was satisfactory for data correction. When the PennPET is expanded to 140 cm, an integrated CT will be installed.

Human Studies:

These studies have been approved by the University of Pennsylvania Institutional Review Board and carried out under IRB #809476 and all study participants signed informed consent. Subjects were required to be ≥ 18 years of age and pregnant women were excluded. Three groups of patients were recruited for this study: healthy volunteers, patients who had clinical PET scans as part of their SOC medical treatment, and subjects participating in other PET research studies with permission of the research study. The overall protocol for each group of patients is described below; details of specific patient studies are provided in the Results section and in Table 1.

All healthy subjects underwent a comparator scan on a commercial PET/CT scanner (Ingenuity TF, Philips Healthcare, Cleveland Ohio). For ^{18}F-fluorodeoxyglucose (FDG), the comparator scan was acquired with SOC clinical parameters (1.5-2 min/bed depending on BMI) about 60 ($\pm$15) min after intravenous administration of ~555 MBq (15 mCi) FDG. The subjects were then escorted to the PennPET where scans were acquired in a single bed position without reinjection of the radiotracer. With 64-cm axial coverage the subjects were imaged from vertex of the head through the abdomen. To simulate scans of shorter duration, list-mode data were subsampled. Delayed images, up to 10 half-lives after injection, were obtained in select patients to study late kinetics and the ability to ability to image at low activity.

To study the potential for dynamic whole-body imaging, two healthy subjects received bolus injections of FDG during imaging on the PennPET. After an hour of dynamic imaging, delayed scans were obtained. For these subjects, the SOC scan was acquired after the dynamic scan on the PennPET. These studies illustrate the wide dynamic range in count rate capability of the instrument that includes capturing the time activity curves for the blood input functions.

After establishing the feasibility of human imaging with the PennPET, clinical patients with disease were imaged after completing their standard of care PET/CT scan. One study utilized FDG with the Ingenuity TF (Philips Medical, Cleveland Ohio), while another study utilized ^{68}Ga-DOTATATE with the Biograph mCT (Siemens Healthineers, Erlangen Germany). Subjects enrolled in separate research studies using investigational radiotracers were also enrolled into this companion study to acquire additional images on the PennPET after the completion of their primary research imaging. One study imaged ^{18}F-nitrous oxide synthase (NOS) (*14*), an imaging agent that targets the inducible form of nitric oxide synthase specific to inflammation; the subject was on the PennPET imaged from the vertex to the lower abdomen 2 hours post-injection. Another study imaged ^{18}F-fluortriopride (FTP), an imaging agent for the dopamine D3 receptor;

PennPET imaging centered on the upper abdomen after consumption of a fatty meal to stimulate gallbladder emptying, as dosimetry studies have demonstrated that the gallbladder wall receives the highest dose (*15*).

RESULTS

We initiated human imaging in August 2018 and during this initial period of evaluation we have imaged ten subjects with four different tracers. Subjects ranged from 154-178 cm in height with BMIs of 19.3-26.5 kg/m^2. The demographics and scan details for all subjects are available in **Table 1**. Images were selected to highlight specific features of this whole-body imager. We describe results for each specific type of study below.

Subject #1 was imaged several times on the PennPET, beginning at 1.5 hr post injection (p.i.) of FDG. The first PennPET scan was 20 min in duration. Data from both the PennPET and the clinical scan were subsampled and reconstructed to emulate shorter scans, or, equivalently, lower activity. Reconstruction parameters were matched on both scanners to allow direct comparison. Image quality for this and subsequent studies was assessed by the (four) co-authors who are experienced clinicians with expertise in reading PET. An image from a 16-min scan, chosen to match the clinical scan duration (for similar axial coverage), is shown in **Figure 1A** along with a subsampled 2-min scan. An image from the clinical scan is shown in **Figure 1C** along with a scan subsampled to 2 min. Qualitatively superior image quality—a combination of less noise and better anatomic detail—is seen in the 16-min PennPET scan compared to the clinical scan; the subsampled 2-min PennPET image demonstrates qualitatively comparable, if not better, image quality than the 16-min SOC clinical scan. In comparison, marked image degradation is seen in the subsampled 2-min clinical scan. The transverse slices of the PennPET data through the liver (**Fig. 1B)** illustrate the low noise and uniformity in the scans from 16 min to as short as 37 s (1/32 subsampled data).

A ten-min FDG-PET scan of subject #2 demonstrates the excellent image quality of the PennPET (**Fig. 2A**), as evidenced by the combination of low noise and structural detail (e.g. the

vertebral bodies and vessel walls), as well as the ability to simultaneously image the brain and body. To fully demonstrate the structural detail of the PennPET, the subject was positioned with the brain centered in the axial FOV for a second scan. The transverse images through the cerebral hemispheres centered at the basal ganglia (**Figure 2B**) demonstrate the high definition of these anatomic structures, as well as the high sensitivity of the instrument. We had previously shown that brain images acquired near the center of the axial FOV do not show evidence of spatial resolution blur compared to images acquired near the edge of the axial FOV, despite the much larger acceptance of oblique lines-of-response (*6*). Combined with the high counts from being centered in the axial FOV, the PennPET could be used to better quantify radiotracer uptake and kinetics in these small structures, which have proven roles in neurologic disease.

Subject #3 was scanned dynamically on the PennPET at 10-40 min p.i. of FDG; additional imaging was obtained out to 18.6 hr p.i. The images in **Figure 3A** and the time-activity curves in **Figure 3B** illustrate the kinetics of normal FDG uptake over the entire imaging interval demonstrating the potential to measure tracer kinetics over more than 10 half-lives of ^{18}F. Blood pool activity decreases over time while FDG uptake in the myocardium increases. The 18.6-hour delayed scan reveals decreased FDG uptake in the brain compared to earlier time points. Washout of FDG at such delayed time points has not been previously observed so clearly in humans. A subacute rib fracture demonstrates expected increased uptake of FDG, which also increases over time relative to normal tissue. Similar kinetics for FDG on delayed images out to 10 half-lives (19 hours p.i.) were also measured for subject #1 (see **Supplemental Figure 1**).

Subject #7, a healthy volunteer, was injected with a rapid bolus of FDG (~ 2 s) inside the PennPET to study the early kinetics of FDG with particular attention to the blood input function. **Figure 4** shows representative time frames in the initial uptake, each 1 s in duration; a movie of

the dynamic scan is seen in **Supplemental Figure 2**. This fine temporal sampling, in combination with the excellent image quality of the PennPET, allows the identification of vascular structures as signal appears within the vessels. For example, the arterial vasculature of the head and neck is seen at 16 s, followed by the venous vasculature at 21 s. **Figure 4B** shows the blood input function measured in several vessels and the left ventricle. These time-activity curves demonstrate the expected path of FDG from the pulmonary artery, to the left ventricle, and into the systemic circulation with low sampling noise. The effects of radiotracer dispersion and partial volume averaging are apparent. Also shown in **Figure 4B** are the time activity curves of major organs, illustrating the ability to measure all simultaneously.

Two clinical patients were scanned on the PennPET following a SOC PET to allow for direct comparison between the scanners. The default clinical reconstruction algorithm was utilized for the SOC PET studies. Subject #5, a patient with metastatic colon cancer, was scanned twice on the PennPET with FDG, before and after initial treatment (**Figure 5**). On both PennPET scans, perihepatic disease is more conspicuous, in part owing to clearance of FDG from the non-diseased adjacent liver. The PennPET also clearly demonstrates an FDG-avid epiphrenic (near the diaphragm) lymph node on the baseline scan that was not identified on the SOC scan.

A clinical patient (subject #8) with metastatic neuroendocrine cancer patient undergoing a ^{68}Ga-DOTATATE PET study was scanned to evaluate imaging a radiotracer with a shorter half-life and lower administered activity compared to FDG ($t_{1/2}$ = 68 min for ^{68}Ga versus 110 min for ^{18}F). The activity at the time of scanning on the PennPET (3.5 hr p.i.) was one-fifth of the activity at the time of the clinical scan (65 min p.i.), effectively corresponding to an injected activity of ~30 MBq. Nonetheless, qualitative inspection of the two scans shown in **Figure 6** demonstrates comparable diagnostic image quality on the PennPET compared to the clinical scan. Given the

high cost and limited availability of ^{68}Ga-DOTATATE, scanning at much lower activity may have practical implication.

Two subjects were scanned on the PennPET following protocol-specific research PET scans with experimental research radiotracers. A representative image (3 min scan) of subject #6 is shown 2 hours after intravenous administration of 222 MBq (6 mCi) ^{18}F-NOS (**Figure 7A)**. Whole-body imaging revealed unexpected ocular uptake in this study, which was excluded from the FOV of the standard research scan.

Subject #9 was injected with ^{18}F-FTP and scanned dynamically for 30 minutes with images centered over the gallbladder (**Fig 7B)**. Representative images (1 min scans) demonstrate mild gallbladder emptying over time underscoring potential uses for the PennPET in dosimetry studies. These research studies demonstrate unique PennPET capabilities for PET research investigation, motivating further studies with these and other radiotracers.

DISCUSSION

Initial human imaging studies on the prototype PennPET Explorer demonstrate the diverse applications of a sensitive whole-body imager. These studies provide proof-of-concept for several of the projected applications of the PennPET (*4,5*). For clinical use, the PennPET can produce higher quality images faster than current commercial scanners or comparable images with a significantly reduced activity. As a research tool, the expanded axial FOV of the PennPET not only allows for greater axial coverage, but also enables dynamic whole-body imaging to benefit kinetic analysis studies. The increased sensitivity afforded by the long axial FOV allows delayed imaging, which may improve lesion detection as well as enable fundamental biological insights.

Initial qualitative comparison shows FDG-PET images from the PennPET are of superior quality compared to the SOC PET when performed with similar scan durations as shown in **Figure 1**. These improvements in image quality translate to better delineation of sites of disease in subject #5 with metastatic colon cancer on the PennPET compared to the SOC scan, noting that the PennPET was performed later (see **Fig. 5)**. Perihepatic disease was more conspicuous on the PennPET images and an epiphrenic lymph node was only visualized with the PennPET. More accurate delineation of disease may have treatment implications for both FDG and other tracers. Beyond oncology, imaging small brain structures may benefit from better count statistics due to the large acceptance angle the PennPET Explorer, as shown in **Figure 2**. It is perhaps more noteworthy that the large axial coverage of the PennPET presents a unique opportunity to study brain-body interactions with dynamic imaging protocols.

Compared to commercially available PET scanners with standard axial FOV, long axial FOV imagers such as the PennPET can produce images of comparable quality in much less time.

The subsampled data from subject #1 demonstrated quality in a 2-min scan on the PennPET comparable to that achieved in 16 min on the clinical scanner. This 8-fold decrease in scan time could increase patient throughput in a busy clinic and aid patient comfort. The images of the liver in **Figure 1** demonstrate low noise and uniformity in subsampled images < 1 min, suggesting that detectability of small lesions would be preserved at very short scan times. Such short scans could be leveraged to obtain breath-hold PET images, which may benefit thoracic imaging (*16*). Furthermore, for pediatric indications, scan times sufficiently short to forego sedation would improve safety and decrease the cost and complexity of imaging (*17*). For specific applications, scan time could be tailored to the clinical need for disease characterization.

Similarly, the increased sensitivity of the PennPET also facilitates scanning lower activities of radiotracer than are typically used without a compromise in image quality. Comparable images were obtained with the PennPET with effectively one-fifth of the DOTATATE activity used for the clinical scan (see **Fig. 6)**. Images with lower activity may prove beneficial for pediatric patients (*18*), as well as for imaging radiotracers with limited supply, including those for research and clinical care. With limited availability of ^{68}Ga from a ^{68}Ge/^{68}Ga generator (*19*) and research efforts to produce ^{68}Ga from a cyclotron, the PennPET may be utilized in specialized centers to maximize clinical availability of this radiotracer. Finally, the increased sensitivity could be used to better image the rare positron from the decay of ^{90}Y (*20*) or the low positron fraction of ^{89}Zr with cell tracking.

The increased sensitivity of the PennPET enables imaging at later time points, exploiting the washout of FDG from normal tissues and trapping in malignancy. This is seen clearly with the perihepatic disease in subject #5. Sensitivity with which lesions are detected may consequently improve (*21*). Similarly, delayed imaging of gliomas improves distinction between tumor and

normal gray matter owing to faster washout of FDG from the gray matter (*7*). Markedly delayed imaging of FDG beyond 10 half-lives with the PennPET was performed with 3 subjects (#1, #3, #7) and clearly demonstrates washout of FDG from the brain providing the most definitive evidence of the existence of the dephosphorylation constant, k_4, in a human image. Spence et al. previously estimated k_4 in gliomas and in normal brain with imaging up to 8 hours (*7*). Berg et. al demonstrated washout from the brain in rhesus monkey studies (*22*). We are currently pursuing kinetic analysis studies to estimate k_4 over the extended period of imaging. For PET dosimetry applications, more accurate delayed scans can give better estimates of behavior of the tail of the time activity curve with resultant improvements in dosimetry estimates. An example of a dosimetry application was shown for ^{18}F-FTP.

Dynamic whole-body scanning with the PennPET can benefit kinetic analysis by simultaneously capturing structures outside of a standard axial FOV, including sites of disease, relevant normal organs, and an input function. As shown in the time-activity curves for subject #7 (see **Fig. 4)**, the fine temporal sampling of PennPET allows relatively noise-free input curves, even capturing recirculation of radiotracer after the initial bolus. Comparison of vessels as radiotracer travels from the heart reveals significant partial volume and dispersion effects. Having the left ventricle always within the FOV provides a validated image-derived input function (*23*), possibly obviating the need for sophisticated correction techniques (*24*) or direct arterial sampling. The inclusion of such an input function could be used to estimate first pass uptake of FDG to estimate tumor perfusion (*25*) and further characterize disease.

There are some limitations to these early human studies on this novel scanner. These studies were performed in a prototype 3-ring configuration. A separate commercial CT was used for attenuation correction necessitating image registration. As mentioned, the PennPET will soon be expanded with additional detector rings for a larger axial FOV, and an integrated CT scanner

will then be installed to improve efficiency and CT co-registration. Quantification of radiotracer uptake at very delayed time points has proved challenging, especially for structures with very low activity relative to background activity. This will require a careful investigation of the accuracy of our data correction methods, especially background correction. Lastly, physiologic changes in subjects over extended periods of time—eating, insulin, exertion—were not controlled in this study, and may confound interpretations of late FDG kinetics.

CONCLUSION

These first human studies of the large axial FOV PennPET Explorer validate the successful implementation of many of the key components of design related to data acquisition and reconstruction of large data sets described in our companion paper (*6*). Both clinical and research examples were provided, underscoring the power and versatility of a sensitive long axial FOV scanner. Future investigations will examine the benefits of the full device with expanded axial FOV, and refine quantitative methods for analysis, optimize imaging protocols, and study novel applications, including dual tracer imaging.

Disclosure: We acknowledge support from NIH R01-CA206187, R33-CA225310, R01-CA113941, and KL2TR001879, as well as the Department of Radiology, University of Pennsylvania, and Philips Healthcare for the development of the PennPET Explorer and the studies presented herein. We also acknowledge support from NIH R01-DA029840 and a TAPITMAT-TBIC grant from the University of Pennsylvania for the research studies included in this manuscript. No other potential conflicts of interest relevant to this article exist.

Acknowledgments: We are grateful for the contributions of Michael Geagan, Tim McDermott, and Matt Werner at the University of Pennsylvania for the development of the prototype, and support from Drs. Chi-Hua Tung and Amy Perkins of Philips Healthcare, and the engineering team from the Philips CT/AMI R&D group. We further thank Dr. Janet Reddin and the Nuclear Medicine clinical research team in the Department of Radiology for helping to perform the human studies, and the PET Center Cyclotron facility for providing the radiotracers. Lastly, we thank our research volunteers who selflessly donated their time for this research.

Key Points

QUESTION: How does larger axial coverage of a PET instrument lead to benefits for human imaging?

PERTINENT FINDINGS: The performance of the prototype configuration of the PennPET Explorer whole-body imager has been evaluated with human studies. The clinical studies demonstrate excellent image quality and potential for imaging with lower activity and shorter scan duration. The studies presented also demonstrate the potential for very delayed imaging and the measurement of multi-organ kinetics.

IMPLICATIONS FOR PATIENT CARE: The high sensitivity and large axial coverage of the PennPET Explorer whole-body imager will lead to benefits for clinical FDG studies and also enable translational research that leverages the ability to measure kinetics in multi-organ systems.

References:

1. Hsu DF, Ilan E, Peterson WT, Uribe J, Lubberink M, Levin CS. Studies of a next-generation silicon-photomultiplier–based time-of-flight PET/CT system. *J Nucl Med.* 2017;58:1511-1518.

2. Reddin JS, Scheuermann JS, Bharkhada D, et al. Performance evaluation of the SiPM-based Siemens Biograph Vision PET/CT system. In: *Conference Record of the 2018 IEEE Nuclear Science Symposium and Medical Imaging Conference*. Sydney, AU: 2018.

3. Rausch I, Ruiz A, Valverde-Pascual I, Cal-González J, Beyer T, Carrio I. Performance evaluation of the Vereos PET/CT system according to the NEMA NU2-2012 standard. *J Nucl Med.* 2019;60:561-567.

4. Cherry SR, Jones T, Karp JS, Qi J, Moses WW, Badawi RD. Total-body PET: maximizing sensitivity to create new opportunities for clinical research and patient care. *J Nucl Med.* 2018;59:3-12.i

5. Cherry SR, Badawi RD, Karp JS, Moses WW, Price P, Jones T. Total-body imaging: transforming the role of positron emission tomography. *Sci Transl Med.* 2017;9:381.

6. Karp JS, Viswanath V, Geagan MJ, et al. PennPET Explorer: Design and preliminary performance of a whole-body imager. *J Nucl Med.* (e-pub June 21, 2019 as doi:10.2967/jnumed.119.229997).

7. Spence AM, Muzi M, Mankoff DA, et al. 18F-FDG PET of gliomas at delayed intervals: improved distinction between tumor and normal gray matter. *J Nucl Med.* 2004;45:1653-1659.

8. Badawi RD, Shi H, Hu P, et al. First human imaging studies with the EXPLORER total-body PET scanner. *J Nucl Med.* 2019;60:299-303.

9. Viswanath V, Daube-Witherspoon ME, Schmall JP, et al. Development of PET for total-body imaging. *Acta Phys Pol B.* 2017;48:1555-1566.

10. Karp JS, Geagan MJ, Muehllehner G, et al. The PennPET Explorer scanner for total body applications. In: *Conference Record of the 2017 IEEE Nuclear Science Symposium and Medical Imaging Conference (NSS/MIC)*. Atlanta, GA: IEEE; 2017.

11. Frach T, Prescher G, Degenhardt C, de Gruyter R, Schmitz A, Ballizany R. The digital silicon photomultiplier—Principle of operation and intrinsic detector performance. In: *Conference Record of the 2009 IEEE Nuclear Science Symposium Conference Record (NSS/MIC)*: IEEE; 2009.

12. Werner ME, Surti S, Karp JS. Implementation and evaluation of a 3D PET single scatter simulation with TOF modeling. In: *Conference Record of the 2006 IEEE Nuclear Science Symposium Conference Record*: IEEE; 2006.

13. Popescu LM, Matej S, Lewitt RM. Iterative image reconstruction using geometrically ordered subsets with list-mode data. In: *Conference Record of the IEEE Symposium Conference Record Nuclear Science 2004*. Rome, Italy: IEEE; 2004.

14. Herrero P, Laforest R, Shoghi K, et al. Feasibility and dosimetry studies for 18F-NOS as a potential PET radiopharmaceutical for inducible nitric oxide synthase in humans. *J Nucl Med.* 2012;53:994-1001.

15. Doot RK, Dubroff JG, Scheuermann JS, et al. Validation of gallbladder absorbed radiation dose reduction simulation: human dosimetry of [18 F] fluortriopride. *EJNMMI Phys.* 2018;5:21.

16. Torizuka T, Tanizaki Y, Kanno T, et al. Single 20-second acquisition of deep-inspiration breath-hold PET/CT: clinical feasibility for lung cancer. *J Nucl Med.* 2009;50:1579-1584.

17. Arlachov Y, Ganatra R. Sedation/anaesthesia in paediatric radiology. *Brit J Radiol.* 2012;85:e1018-e1031.

18. Gelfand MJ, Parisi MT, Treves ST. Pediatric radiopharmaceutical administered doses: 2010 North American consensus guidelines. *J Nucl Med.* 2011;52:318-322.

19. Cutler CS, Minoshima S. Shortage of germanium-68/gallium-68 generators for the production of gallium-68. In: Zadecky DMaD, ed. Society of Nuclear Medicine and Molecular Imaging: Journal of Nuclear Medicine; 2018.

20. D'arienzo M, Chiaramida P, Chiacchiararelli L, et al. 90Y PET-based dosimetry after selective internal radiotherapy treatments. *Nucl Med Commun.* 2012;33:633-640.

21. Kubota K, Itoh M, Ozaki K, et al. Advantage of delayed whole-body FDG-PET imaging for tumour detection. *EJNMMI.* 2001;28:696-703.

22. Berg E, Zhang X, Bec J, et al. Development and evaluation of mini-EXPLORER: A long axial field-of-view PET scanner for nonhuman primate imaging. *J Nucl Med.* 2018;59:993-998.

23. Gambhir SS, Schwaiger M, Huang S-C, et al. Simple noninvasive quantification method for measuring myocardial glucose utilization in humans employing positron emission tomography and fluorine-18 deoxyglucose. *J Nucl Med.* 1989;30:359-366.

24. Zanotti-Fregonara P, Chen K, Liow J-S, Fujita M, Innis RB. Image-derived input function for brain PET studies: many challenges and few opportunities. *J Cereb Blood Flow Metab.* 2011;31:1986-1998.

25. Mullani NA, Herbst RS, O'Neil RG, Gould KL, Barron BJ, Abbruzzese JL. Tumor blood flow measured by PET dynamic imaging of first-pass 18F-FDG uptake: a comparison with 15O-labeled water-measured blood flow. *J Nucl Med.* 2008;49:517-523.

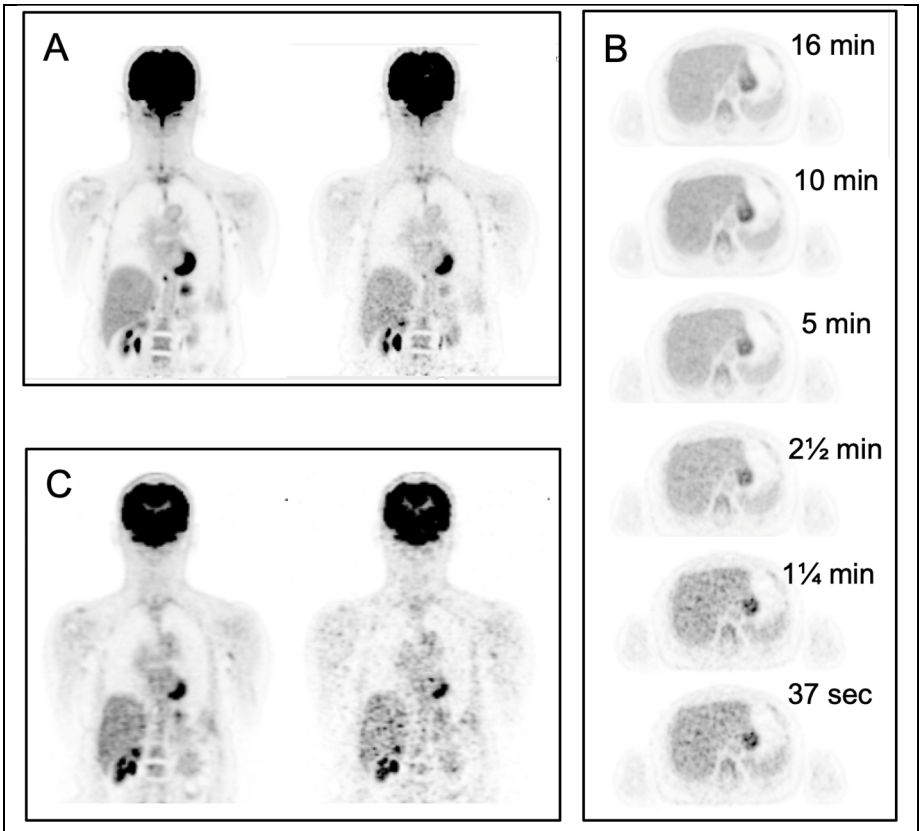

FIGURE 1: A) FDG-PET coronal images of subject #1 on PennPET Explorer acquired at 1.5 hr p.i. of FDG for 16 min (left) and 2 min (right). **B**) Transverse images of liver from PennPET over a range of scan durations. **C**) Coronal images from SOC clinical PET acquired at 0.75 hr p.i. for 16 min (left) and 2 min (right).

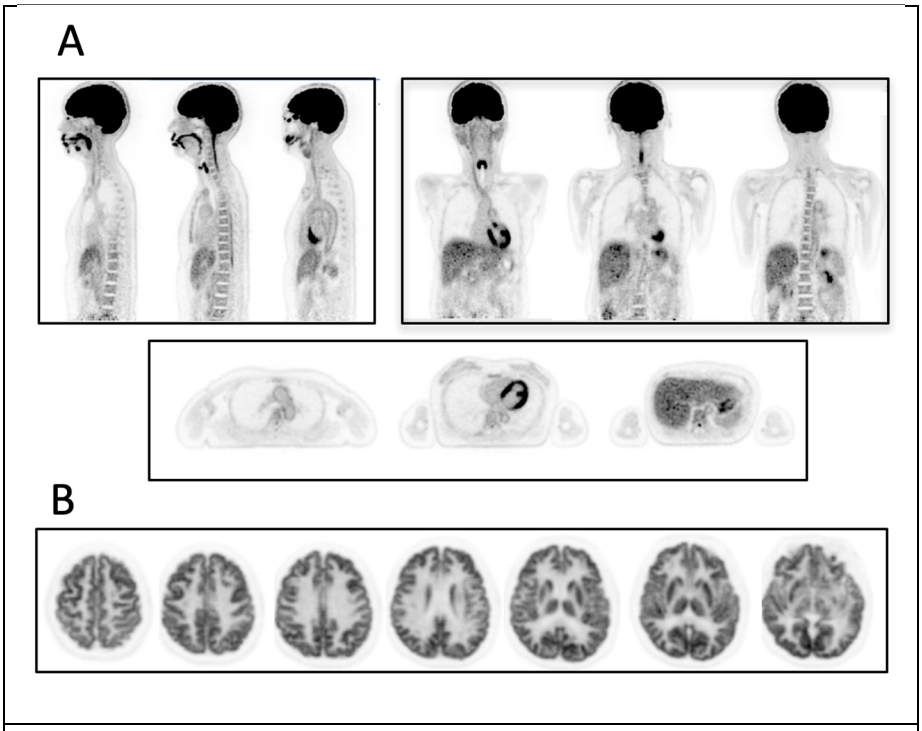

FIGURE 2: A) FDG-PET images of subject #2 (sagittal, coronal, and axial) on PennPET (10 min scan). **B)** Transverse images on PennPET after the subject was moved so that the brain was positioned in center of the axial FOV (10 min scan).

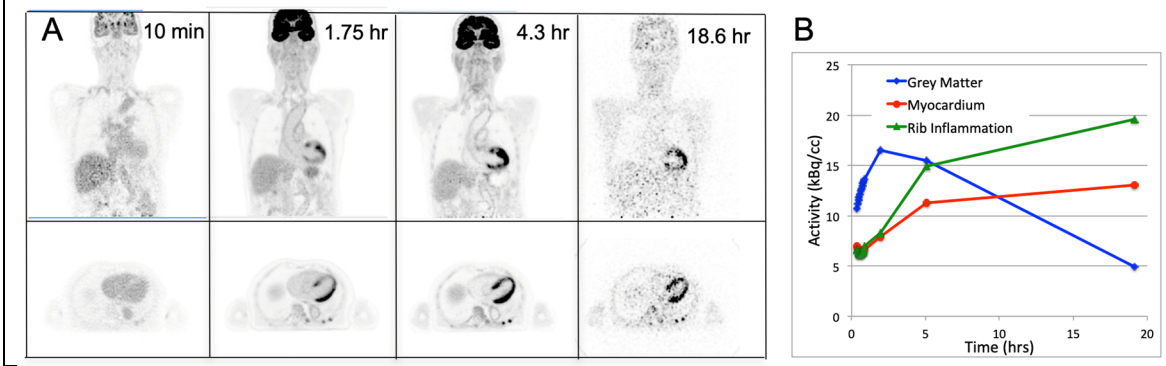

FIGURE 3: A) FDG-PET coronal images of subject #3 acquired at four time points following injection; the first time point is a 3 min scan, whereas other time points have scan durations noted in Table 1. **B)** Time-activity curves (TACs) for brain, myocardium, and a rib fracture from the same patient. The plotted points are at the mid-time of each scan.

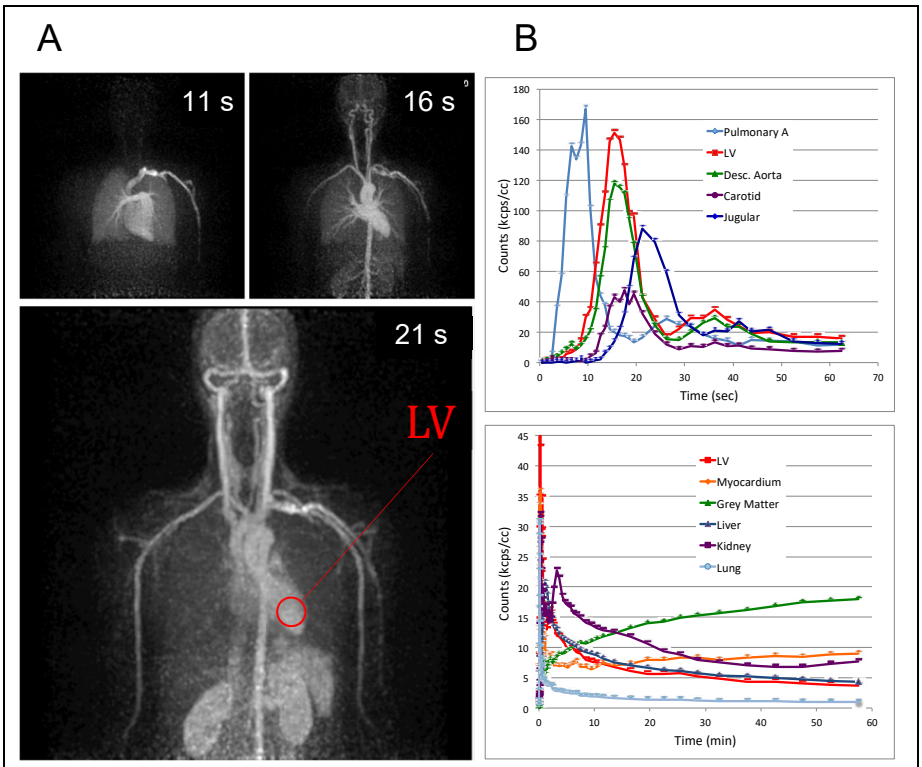

FIGURE 4: A) FDG-PET maximum intensity projection (MIP) images of subject #7, each 1 s in duration, at three time points from a dynamic scan. **B)** TACs of blood input function measured at several vessels over first minute after injection, and TACs of major organs over first hour after injection.

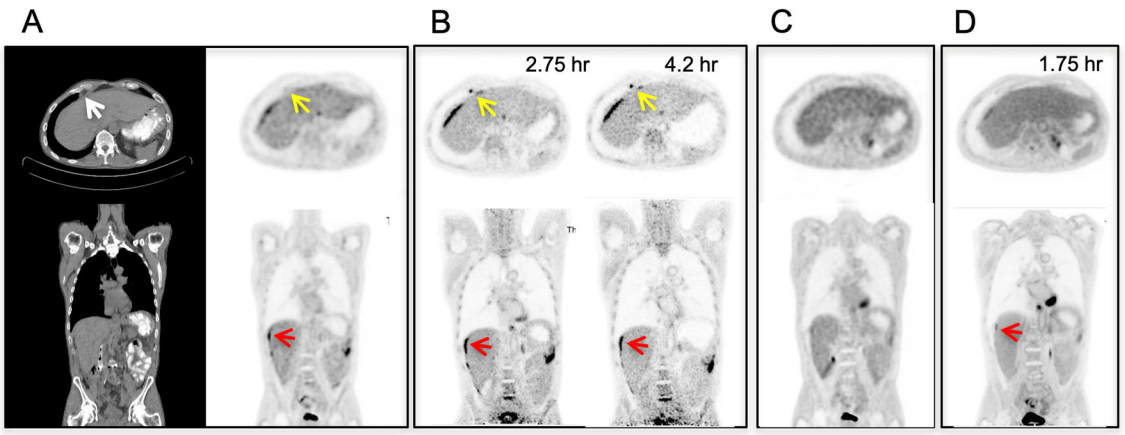

FIGURE 5: Clinical FDG PET/CT images (transverse and coronal) from subject #5 with metastatic colon cancer acquired with standard clinical protocol. **B)** PennPET Explorer image acquired 2.75 hr and 4.2 hr p.i., (10 min scans). Matched coronal and transverse slices are shown. Red arrows denote perihepatic disease; yellow arrows denote the epiphrenic lymph node. **C)** Follow-up clinical scan at 3 mo. (subject #10) and **D)** corresponding PennPET image (20 min scan) demonstrates improvement in perihepatic disease and epiphenic lymph node.

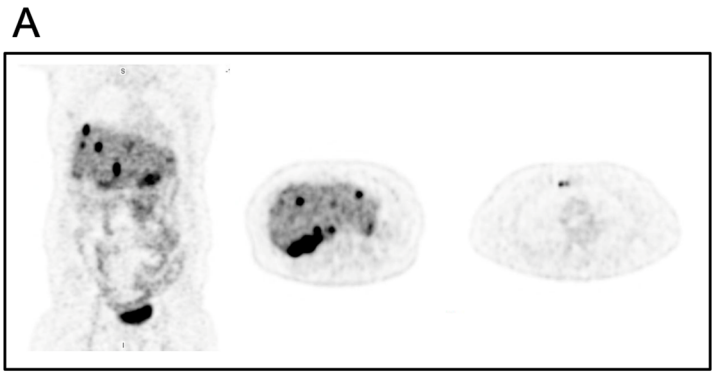

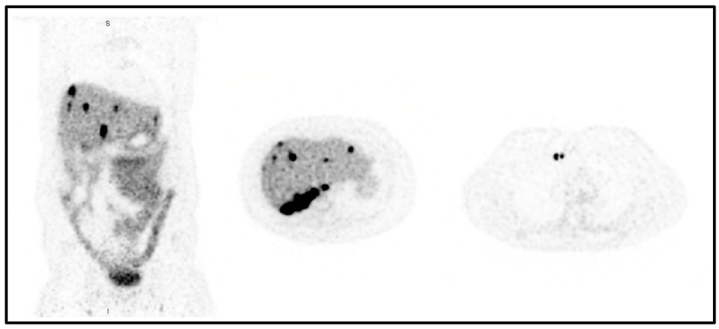

FIGURE 6: A) SOC ^{68}Ga-DOTATATE-PET images (coronal and transverse) of subject #8, a clinical patient with metastatic neuroendocrine tumor. **B)** Coronal and transverse images from the same patient on PennPET acquired 3.5 hr p.i. (20 min scan).

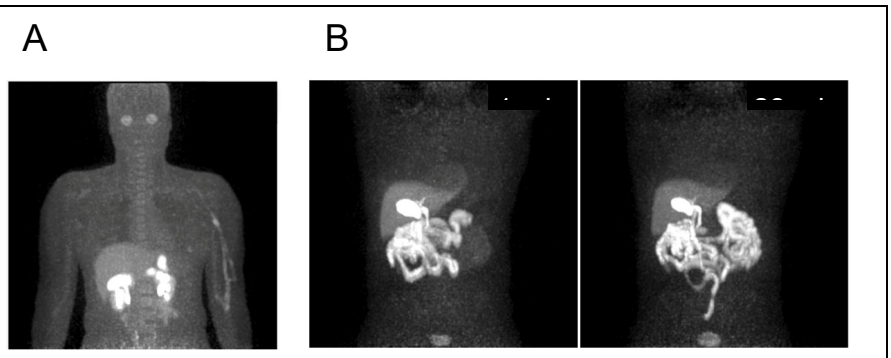

FIGURE 7: A) MIP image (3 min scan) of ^{18}F-labeled nitrous oxide synthase (^{18}F-NOS) PET (subject #6). **B)** MIP images of ^{18}F-fluortriopride (^{18}F-FTP) PET (subject #9) for 1-min duration shown at 1 min (left) and 28 min (right) after drinking Ensure to stimulate emptying of radiotracer from the gallbladder.

TABLE 1: Human subject and study details

#	Age/Gender	Subject Type	BMI (kg/m^2)	Height (cm)	Tracer	Injected Activity (MBq)	PennPET Scan Uptake Time (scan duration)	Clinical Scan Uptake Time (scan duration)
1	62/F	Normal Volunteer	26.5	164	^{18}F-FDG	577	**1h 27m (20m)** **3h 10m (20m)** **5h 14m (20m)** **7h 17m (30m)** **9h 5m (30m)** **18h 50m (60m)**	**45m (20m)**
2	56/F	Normal Volunteer	21.6	154	^{18}F-FDG	559	**1h 33m (10m)** 5h 0m (15m)	57m (15m)
3	79/M	Normal Volunteer	22.9	170	^{18}F-FDG	551	**10 – 40m [dyn]** **1h 44m (20m)** **4h 21m (30m)** **18h 40m (60m)**	1h 9m (15m)
4	79/M	Normal Volunteer	23.3	170	^{18}F-FDG	518	0 – 60m [dyn] 2h 23m (20m) 4h 52m (25m)	N/A
5	60/M	Clinical Patient	20.1	173	^{18}F-FDG	496	**2h 46m (10m)** **4h 12m (10m)**	**60m (15m)**
6	28/M	Research Subject	23.7	163	^{18}F-FNOS	218	**1h 39m (30m)**	0-60m [dyn]
7	29/F	Normal Volunteer	19.3	177	^{18}F-FDG	500	**0 – 60m [dyn]** 2h 13m (20m) 4h 57m (30m) 23h 2m (60m)	3h 0m (15m)
8	58/F	Clinical Patient	25.5	162	^{68}Ga-DOTATATE	152	2h 21m (20m) **3h 32m (20m)**	**1h 5m (10m) ***
9	48/M	Research Subject	26.3	178	^{18}F-FTP	226	**2h 31m – 59m [dyn]**	0-120m [dyn]
10	60/M	Clinical Patient	20.3	175	^{18}F-FDG	555	**1h 46m (20m)** 4h 7m (30m)	**1h 2m (15m)**

PennPET scans included in the manuscript are **bold**. The total scan duration for these studies is listed, although some of the images presented represent shorter scans by subsampling the data.

* Denotes that Siemens Biograph mCT was used as the clinical scanner. All other clinical scans were performed on Philips Ingenuity TF PET/CT.

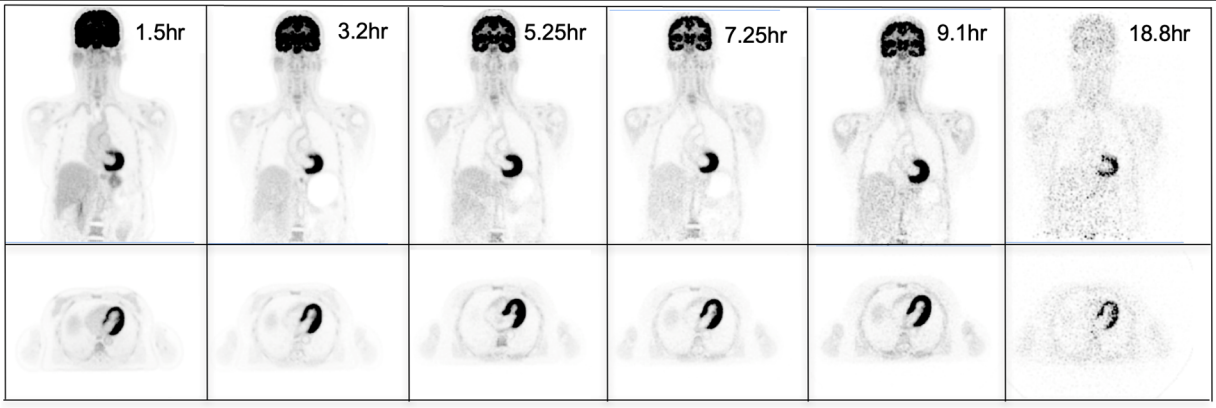

Supplemental Figure 1: FDG-PET coronal images of subject #1 at multiple times p.i.; note variable scan durations as detailed in Table 1.

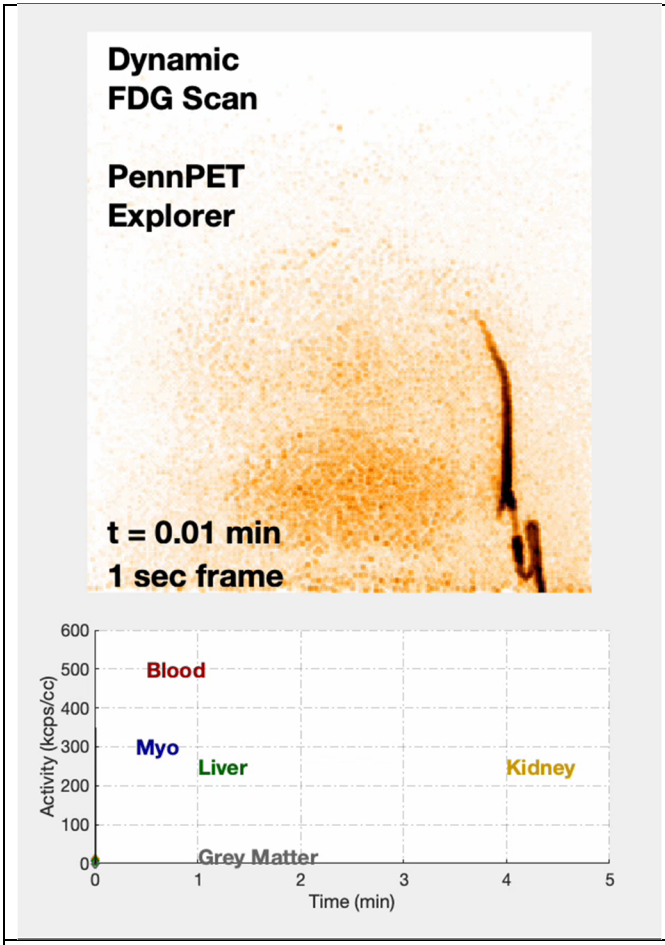

Supplemental Figure 2: Dynamic study of subject #7 injected with fast bolus of FDG and scanned for 1 hour. Movie of multi-frame reconstructed images includes 70 frames ranging from 1 s to 5 min. Also shown are time-activity curves of blood input function and major organs.